Chapter

Challenges and Perspectives for SIW Hybrid Structures Combining Nanowires and Porous Templates

Vivien Van Kerckhoven, Luc Piraux and Isabelle Huynen

Abstract

The chapter presents a review of properties and applications of a particular category of Substrate Integrated Waveguide (SIW) named NWSIW, for NanoWire-based Substrate Integrated Waveguide. The NWSIW topology combines metallic nanowires embedded in a porous template in order to form planar compact integrated waveguides; nanowires selectively grown in the template are used for building the walls of the waveguide, but also allow to achieve microwave functionalities such as filtering, isolation. Through the chapter the comparison made with classical waveguides including SIW will lead to a discussion on future perspectives and possible improvements of this NWSIW topology. Their performances will be explained and illustrated with regards to current state-of-the art, and based on results obtained at UCLouvain.

Keywords: SIW, porous template, metallic nanowires, microwaves, isolator, filter, design, fabrication

1. Introduction

High-quality transmission lines become mandatory to fulfill the requirements of the nowadays applications. Indeed, the constraints applied to microwave and millimeter-wave circuits are continuously reviewed and increased: low cost, low consumption, high density, high operational frequency, … At frequencies higher than 30 GHz, interferences, radiation and material losses prevent the use of conventional microstrip and coplanar transmission lines. Within this context, the substrate integrated waveguide (SIW) topology, introduced in [1], represents a promising perspective. This technology uses two rows of vertical metallic wires or metallized via holes inserted throughout the substrate entire height to form a shielded line of rectangular section, reducing subsequently radiation and conductor losses. The presence of walls also prevents spurious crosstalk interferences between devices in a same circuit [2–4].

The two virtual walls have to be carefully placed to allow the appearance of the same propagation modes as in a macroscopic rectangular waveguide. It is possible to integrate various components in a same substrate, including passive or active devices, as well as antennas. Different variations of the concept emerged for several functionalities (filter, coupler, antenna power supply, …) with applications up to 180 GHz, and in different types of substrates (PCB, paper, polymers or alumina) [5, 6].

Over the last decades also, the interactions between nanowires embedded in porous templates and microwave signals have been intensively studied and exploited to create planar monolithic devices. Both the permeability and permittivity of the template filled with nanowires can be modulated in order to create various microwave and millimeter-wave components. The advantages of microwave devices based on nanowires compared to classical components are manifold: wide range of operating frequencies, temperature stability, monolithic integration into a single substrate and possible miniaturization. Moreover, compared to classical ferrites, ferromagnetic nanowire arrays display higher saturation magnetization and ferromagnetic resonance (FMR) frequencies as well as high operation frequencies at remanence due to their large aspect ratio.

Thanks to those properties, noise suppressors [7], absorbers [8, 9], inductors [10], or filters based on electromagnetic bandgap effect [11] have been developed, together with non-reciprocal devices, such as phase shifters [12], isolators [13] and circulators [14]. More recently slow-wave transmission lines were designed exploiting the high permittivity of metallic nanowire arrays [15], while a filter was designed using the double ferromagnetic resonance effect in magnetic nanowires [16]. The reported devices use microstrip or coplanar waveguide topologies combined with different ferromagnetic materials for the nanowires.

Given the respective advantages of nanowires and SIW [17–19], using nanowires to conceive Substrate Integrated Waveguide (SIW) devices is an interesting alternative. The basic idea underlying this concept is to use metallic nanowire arrays electrodeposited into a porous template to form the waveguide walls. With two copper layers deposited onto the template's both faces, a simple rectangular waveguide is created, denoted NWSIW for nanowire-based substrate integrated waveguide. To achieve different microwave functionalities, various nanowire arrays can be added inside the cavity of the NWSIW, combining different heights, shapes and materials (magnetic or not).

Concepts presented in this chapter are widely inspired by the work of Van Kerckhoven et al. [17–22]. The chapter is organized as follows; Section 2 introduces the Nanowired-based Substrate Integrated Waveguide (NWSIW) topology and compares it with the classical SIW and metallic rectangular waveguide (MRW) geometries. Section 3 details the design features of the NWSIW, while Section 4 discusses fabrication techniques. Section 5 presents some experimental realizations of microwave devices based on NWSIW topology, while Section 6 discusses challenges and perspectives of this new technology.

2. Geometries in presence

Figure 1 shows the transformation of a classical metallic rectangular waveguide (MRW) into an SIW, next into a NWSIW.

The MRW is formed by the assembly of four metallic plates acting as perfect electric conductors and forming a hollow metallic pipe of rectangular section for the guidance of electromagnetic waves.

The SIW has a fully planar thin topology since it bases on planar dielectric substrates commonly used for the fabrication of RF and microwave devices and circuits. The top and bottom faces of the substrate are covered by a metallic clad typically 17 or 35 μm-thick, as available for commercial copper clad laminates (CCL). These layers form the top and bottom walls of the waveguide. Lateral walls are obtained by

DOI: http://dx.doi.org/10.5772/intechopen.105148

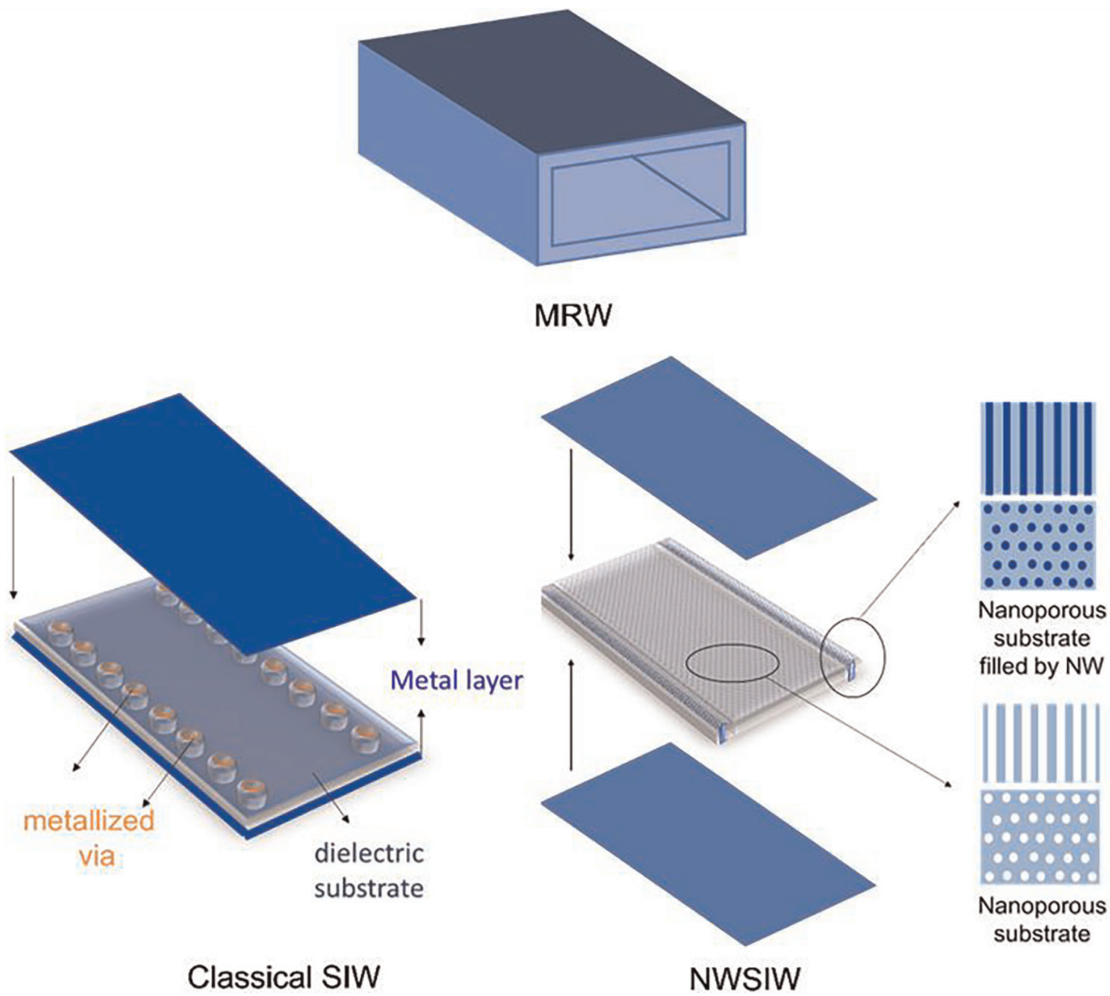

Figure 1.
From metallic rectangular waveguide (MRW) to Nano-wire substrate integrated waveguide (NWSIW). In SIW lateral metal plates of MRW are replaced by two rows of metallized vias. In NWSIW rows of nanowires (NW) electrodeposited in nanoporous substrate form continuous metallic walls. Vertical arrows indicate the positioning of covering metal plates (blue).

mechanically drilling two rows of holes that are next filled by metallic vias; periodicity and diameter of the vias must be adjusted in order to achieve a similar metallic shielding level as in an MRW.

In a NWSIW the difference with respect to SIW is the nanoporous substrate used for its design and fabrication. Instead of drilling vias in a CCL substrate, metallic nanowires (NW) are grown by electrodeposition in dedicated row areas in the nanoporous substrate in order to form a virtual metallic lateral shielding. The bottom side of the waveguide is formed by the thin metallic layer electroplated as ground electrode for the electrodeposition of NW, while top side is achieved by another electroplating realized after the growth of NW is completed.

3. Design rules and constraints for NWSIW

3.1 Alumina porous template

The template considered for the NWSIW is nanoporous alumina wherein metallic nanowires can grow. Commercial solutions are based on anodic alumina oxide (AAO);

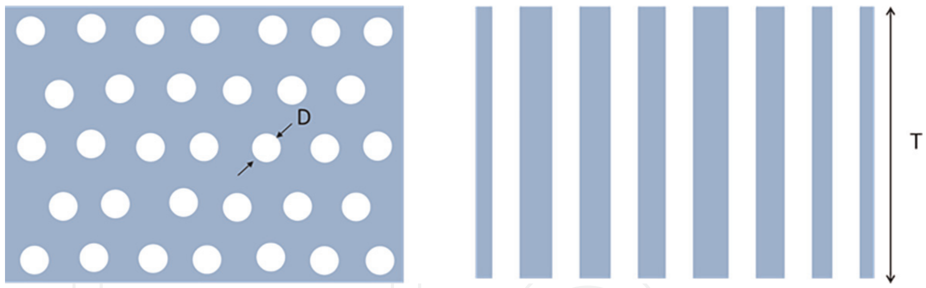

Figure 2.
Schematic top view (left) and side view (right) of AAO template. T is the thickness of the template, D is the diameter of the pores.

Pore diameter range D	30 nm – 1 um
Type and conductivity of NW	Cu - 5.65 x 10^7 S/m
Porosity range (P)	4% - 60%
Dielectric constant bulk alumina (ε_r)	9.8
Relative permeability bulk alumina (μ_r)	1
Loss tangent factor bulk alumina (tanδ)	0.015
Thickness T	50 µm or 100 µm
Operational frequency range	1 GHz – 50 GHz

Table 1.
Characteristics of AAO porous template.

the oxide is obtained by anodization of aluminum. The result is an array of vertical cylindrical pores arranged as a hexagonal pattern, as illustrated in **Figure 2**. The diameter of the pores is fixed by the process and typically ranges between 25 nanometers and 0.5 µm. Another characteristic parameter is the porosity P of the template, defined as the total surface occupied by pores in a given area reported to the surface of this area. The available thicknesses of the AAO template and its electrical parameters are also reported in **Table 1**.

3.2 Building of NWSIW walls

Contrarily to classical a SIW where walls are created by the insertion of metallic vias, the NWSIW architecture exploits the nanoporous nature of AAO to grow arrays of metallic nanowires (MNW) inside pores. Instead of bulk metal for classical RW having bulk conductivity σ, each wall of the NWSIW formed by the nanowire array has a total equivalent conductivity reduced by a factor P [20]. As a consequence, the skin depth δ_{NW} of the nanowire array expresses as

$$\delta_{NW} = \frac{2}{\omega \mu P \sigma} \tag{1}$$

The extinction thickness ET is here defined as the thickness of the nanowire array forming the MNW wall that ensures that 99.9% of the electromagnetic field is blocked/attenuated by the MNW wall:

$$0.001 = e^{-ET/\delta_{MNW}} \rightarrow \mathrm{ET} = 7\,\delta_{\mathrm{MNW}} \quad (2)$$

Figure 3 shows the extinction thickness ET as a function of porosity, for different values of operating frequency, from DC up to 50 GHz, and for Copper (Cu) nanowires of conductivity given in **Table 1**. It is concluded that a thickness of 10 μm is sufficient to satisfy condition (2) for most values of porosity higher than 3% and frequency above 1 GHz.

Practically two rows of MNW are grown in the AAO template, having a 10 μm width and a length equal to the desired length of the NWSIW. The nanoporous AAO template imposes a close packing of the electrodeposited MNW array from which an efficient shield is obtained. This is different and easier than designing the diameter and spacing of metallic vias drilled in the dielectric substrate of classical SIWs.

3.3 Propagation in NWSIW

In this section the propagation of microwave signals is investigated through the description of the effective medium present in the waveguide, as influencing the propagation, and the formulation of the propagation constant and characteristic impedance of the waveguide.

3.3.1 Effective medium filling the NWSIW

The porous medium resulting from alumina anodization was illustrated in **Figure 2**. The (complex) permittivity of the equivalent effective medium, noted ε_{AAO}, can be calculated using a simple volumetric law [20] involving porosity P of AAO and properties of bulk alumina reported in **Table 1**:

$$\varepsilon_{AAO} = P + (1 - P)\varepsilon_r\,(1 - i\,tan\delta) \quad (3)$$

As illustrated in **Figure 4**, both dielectric constant (left figure) and loss tangent factor (right figure) of porous AAO show a linear dependence on porosity P.

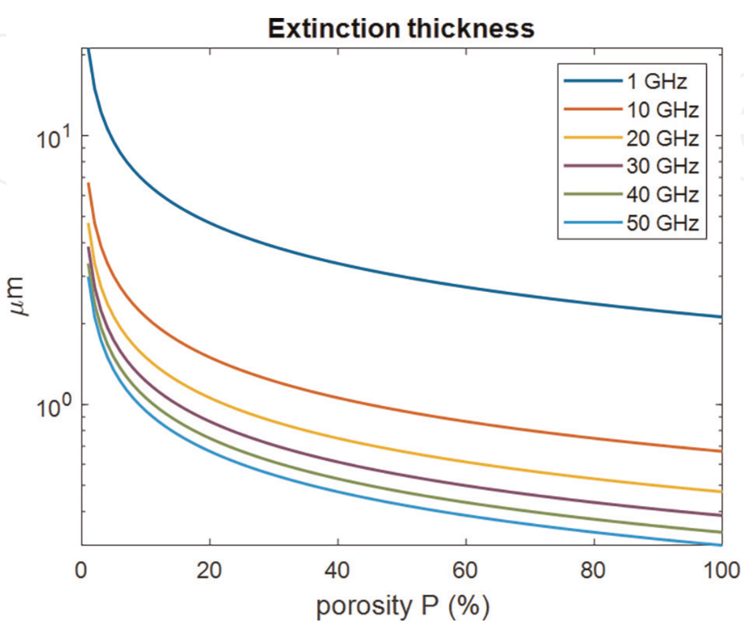

Figure 3.
Extinction thickness (Eq. (2)) as a function of porosity P.

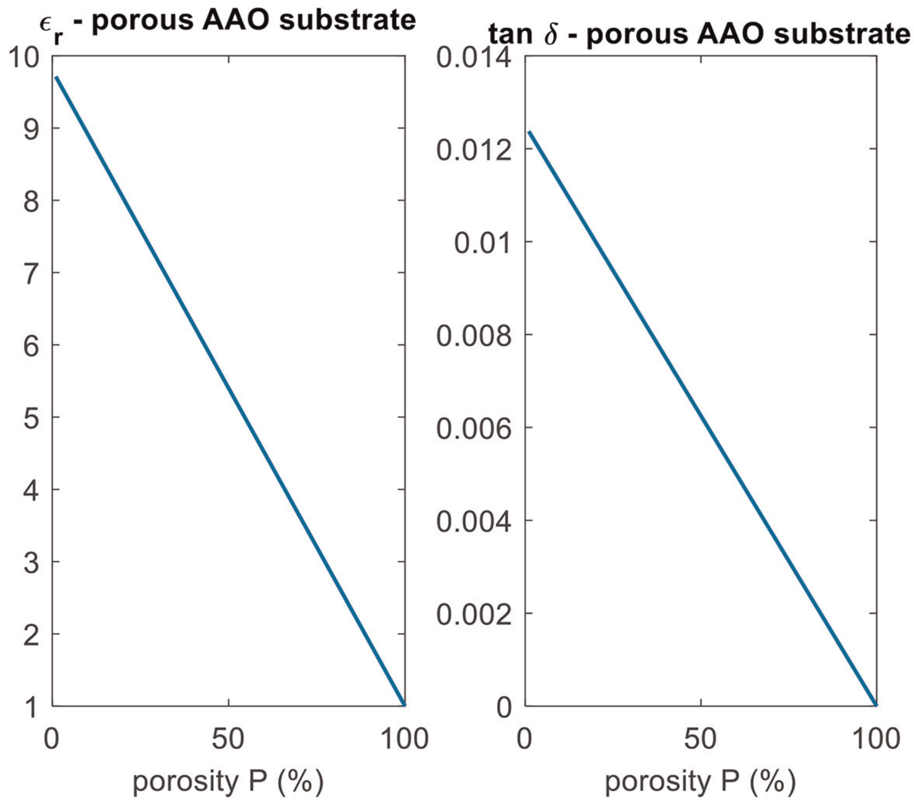

Figure 4.
Electrical properties of porous AAO depending on porosity P, according to Eq. (3). Left: Dielectric constant, right: Loss tangent factor.

For P = 0, the dielectric constant is that of bulk alumina given in **Table 1**, while for P = 100% it corresponds to air since no more alumina is present.

The same is true for the loss tangent factor; it goes from 0.0125 for P = 0%, corresponding to the value in **Table 1** for bulk alumina, to zero since for P = 100% the substrate reduces to air having no significant losses.

It has to be noted however that for practical use, AAO templates having high porosity should be avoided since they are much more brittle.

3.3.2 Propagation characteristics

The propagation inside a NWSIW is very similar to that occurring in a classical MRW. Given its width noted W and height equal to the thickness T of AAO template given in **Table 1**, the complex propagation constant, noted γ, is given by the following general expression [23]:

$$\gamma = \alpha + j\,\beta = \sqrt{\left(\frac{n\,\pi}{W}\right)^2 + \left(\frac{m\,\pi}{T}\right)^2 - \varepsilon_{AAO}\left(\frac{2\,\pi f}{c_o}\right)^2} \qquad (4)$$

In Eq. (4) m and n are indices associated to TE_{mn} and TM_{mn} modes of propagation in an MRW. In the case of NWSIW, the thickness of the AAO being much lower than the width W of the guide, the first modes of propagation are TE_{m0} modes. Eq. (4) indeed reveals that the propagation constant presents a cut-off phenomenon; propagation occurs (β > 0) only above a certain frequency named cut-off frequency and noted f_c. Below f_c, the signal is attenuated instead of propagating (β = 0, α > 0).

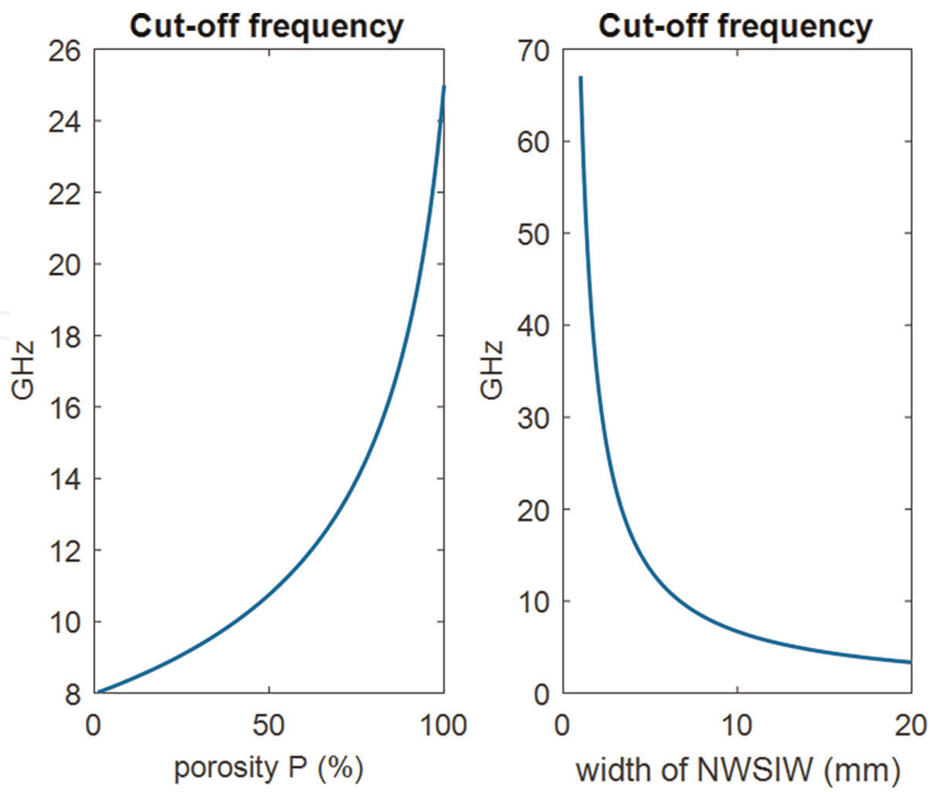

Figure 5.
Cut-off frequency f_{c10} according to Eq. (5). Left: Function of porosity P, for W = 6 mm. Right: Function of NWSIW width W, for P = 50%.

Derived from setting γ in Eq. (4) equal to zero, f_c writes as:

$$f_{c\ m0} = \frac{m\ c_o}{2\ W\ \varepsilon_{AAO}} \quad (5)$$

where W is the width of the waveguide and c_o the light velocity in air. For the NWSIW the three lowest cut-of frequencies occur for TE_{m0} modes.

Two statements can be derived. At first, the permittivity of AAO filling the waveguide depends on porosity P. This obviously influences the cut-off, hence the propagation constant, by virtue of (4–5). This illustrated in **Figures 5** and **6**, left. As porosity P increases, the dielectric constant decreases so that cut-off moves to higher frequencies (**Figure 5**), and this is reflected in the behavior of propagation constant (**Figure 6**). For a proper operation, that is allowing propagation in the 10–60 GHz range, porosity P should not exceed 40%.

Secondly, similar conclusions can be drawn as concerns the influence of the width of the waveguide. The cut-off frequency decreases as the width of the NWSIW increases, and a width superior to 5 mm is necessary for obtaining propagation in the NWSIW starting at 10 GHz.

3.3.3 Characteristic impedance of NWSIW

The characteristic impedance of a NWSIW has an expression similar to an MRW, expressed here as function of geometrical parameters W and T of the waveguide [23]:

$$Z_c = \frac{2\ T}{W}\ \frac{j\ 2\pi f\ \mu_o}{\gamma} \quad (6)$$

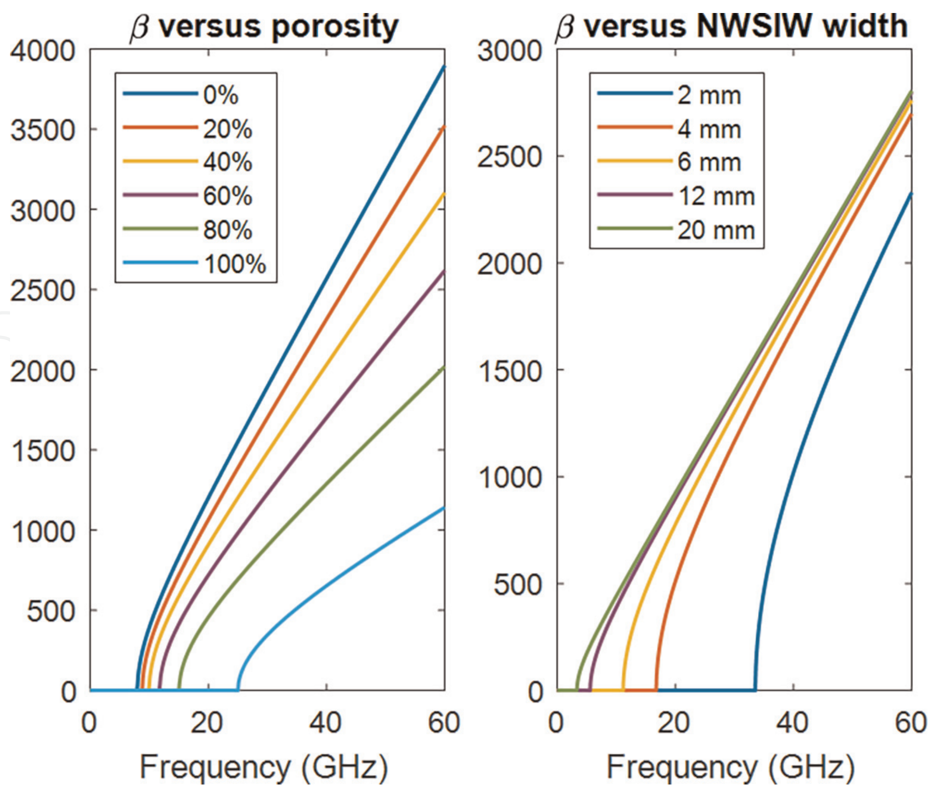

Figure 6.
Frequency dependence of propagation coefficient β given by Eq. (4). Left: For different values of porosity P, and W = 6 mm. Right: For different values of NWSIW width W, and P = 50%.

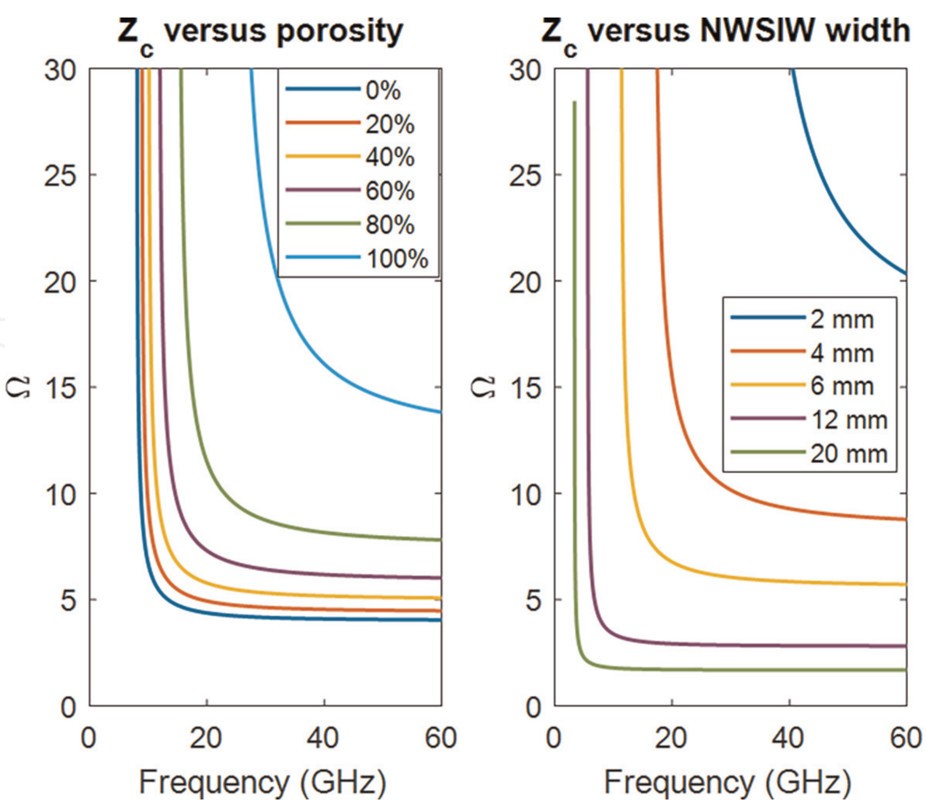

Figure 7.
Frequency dependence of characteristic impedance Z_c given by Eq. (6). Left: For different values of porosity P, and W = 6 mm. Right: For different values of NWSIW width W, and P = 50%.

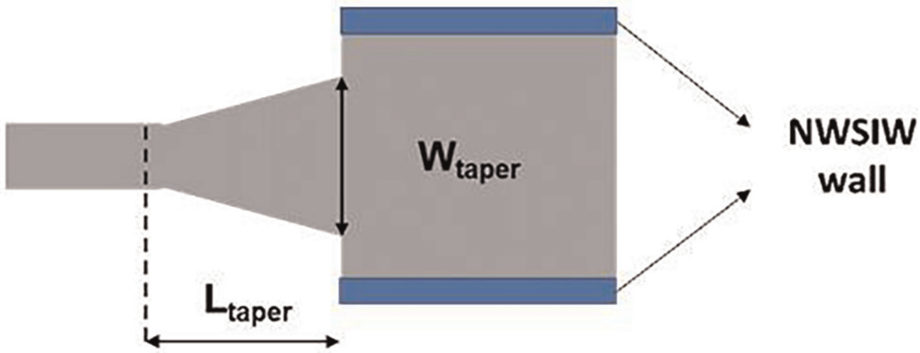

Figure 8.
Schematic representation of tapered microstrip-to-NWSIW transition for impedance matching.

Introducing expression (4) of γ into (6), the characteristic impedance Z_c can be represented in **Figure 7** as a function of frequency and for different values of porosity (left) and width of NWSIW (right). Resulting from definition (6) Z_c has a singularity at cut-off frequency, since at this frequency γ present in the denominator of (6) tends to zero.

Another important feature is the low level of characteristic impedance far above cut-off. Even for the most favorable conditions, i.e. high porosity in order to decrease the effective permittivity inside the waveguide (P = 80%), and moderate width of NWSIW (W = 4 mm), Z_c does not exceed 10 Ω in the flat constant regime above 20 GHz. As a result, a mismatch occurs with respect to the conventional 50 Ω reference impedance used for measurements of microwave devices.

3.3.4 Tapered transmission for improved matching

As a way to solve the problem of mismatch between the low impedance of the NWSIW and 50 Ω reference impedance, tapered transitions can be inserted between accesses of the NWSIW and microstrip or coplanar waveguides lines used for the connection with other devices. A schematic view of the microstrip-to-NWSIW transition is shown in **Figure 8**. The taper allows a smooth progressive change of characteristic impedance along taper length, which favors the matching.

Figure 9 shows simulated performances of microstripline -to - NWSIW transition for various values of taper length $L = L_{taper}$ (left) and taper width W_{taper} (right).

Adequate values for maximizing transmission S_{21} and minimizing reflection S_{11} are $L_{taper} = \lambda/4$ where λ is the wavelength at the operating frequency assumed here equal to 10 GHz, and $W_{taper} = 0.6 \times W = 3.6$ mm.

4. Fabrication techniques

Figure 10 shows the fabrication process for the NWSIW. As explained in Section 2, this technology differs from classical SIW since it takes advantage of the porous AAO template for creating by electrodeposition metallic nanowires inside the pores in order to form equivalent metallic shielding walls as explained in sections 3.1 and 3.2.

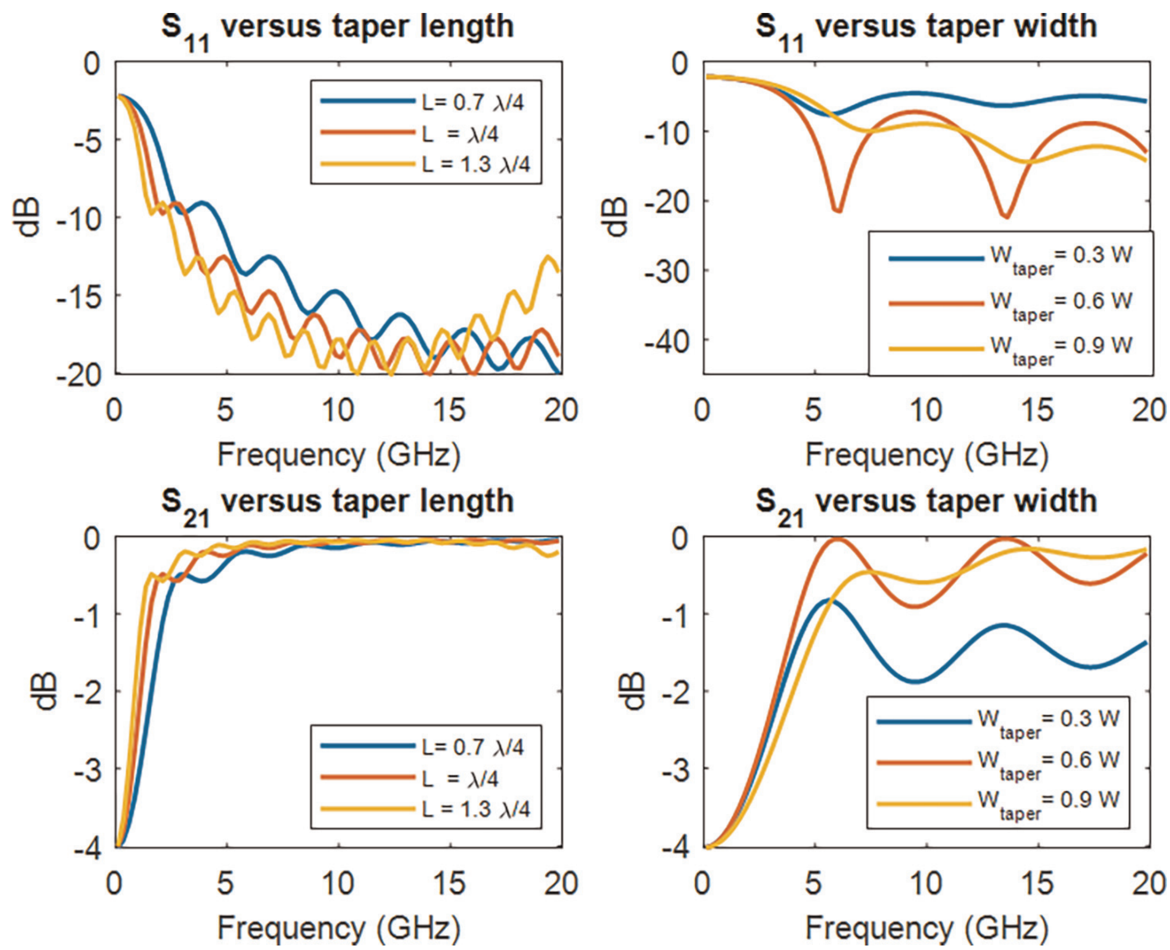

Figure 9.
*Performances of tapered transition of **Figure 8** as a function of taper length (left) and taper width (right). Top row: S_{11}, bottom row: S_{21}. Simulations are made for W = 6 mm and P = 50%.*

The first step is the deposition of a metallic layer (blue color) by electroplating on the back side of the AAO template, step 1 in **Figure 10**; this layer is used as cathode during the electrodeposition process.

Then in step 2 the areas where electrodeposition of NW is needed are defined; equivalently the areas where electrodeposition is unwanted are determined. As detailed in [19–21] two options are possible, named A and B. In option A, a metal layer is electroplated on top of AAO. Openings are created by laser etching this top metal layer in areas where electrodeposition of MNW is desired, to allow the penetration of the electrolytic solution inside pores that are not covered by the metal. Option B is dual/opposite; the areas where MNW are unwanted are selected by laser burning locally the surface of the AAO in order to destroy locally the porosity and clog the pores, making electrodeposition of MNWimpossible in these areas. The burned surface of AAO is represented as a magenta layer in **Figure 3B**. It remains present during step 3 to 5. The result of step 2 for both option A and B is step 3, where only open pores are available for electrode-position. The result of step 2 for both option A and B is step 3, where only open pores are available for electrodeposition.

The last 2 steps are similar for option A and B. In step 4, electrodeposition process described in [21] is used to grow MNW in free pores in such a way that pores are slightly overfilled. By doing so, during step 5 when electroplating of top metal layer occurs, good electrical contacts are created between top metal layer and

DOI: http://dx.doi.org/10.5772/intechopen.105148

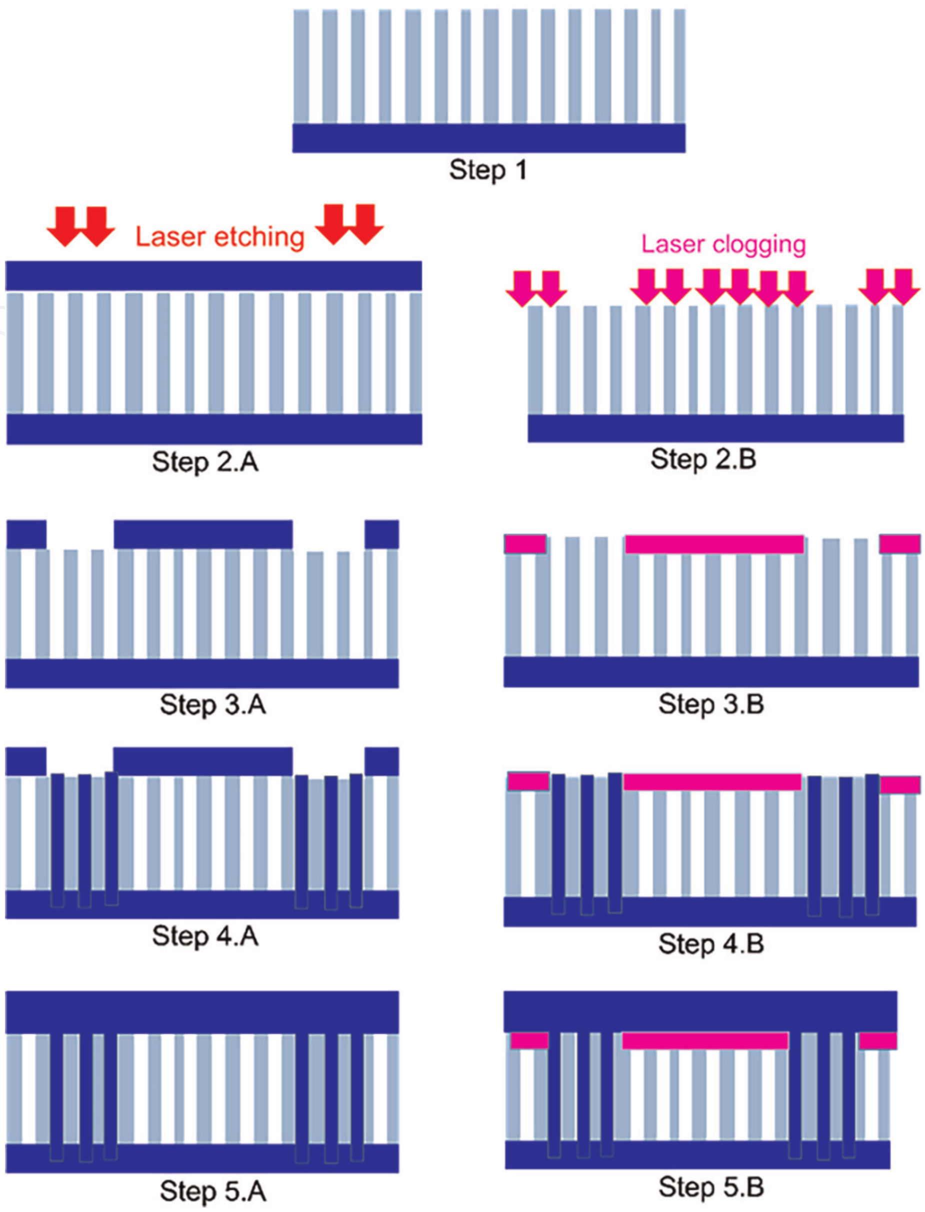

Figure 10.
Steps of fabrication process for the NWSIW.

upper end of MNW, forming efficient metallic shielding walls for the equivalent waveguide.

5. Practical realizations

5.1 NWSIW transmission line

Figure 11 shows the transmission measured in a NWSIW transmission line having a width W = 6 mm, and built on a 100 μm-thick AAO template. The location of the three first cut-off frequencies corresponding to TE_{10}, TE_{20} and TE_{30} modes are visible; their values are in good correspondence with Eq. (5). For a proper operation of NWSIW devices, they should be designed for the 8–18 GHz frequency range, i.e. between the first and second cut-off frequencies.

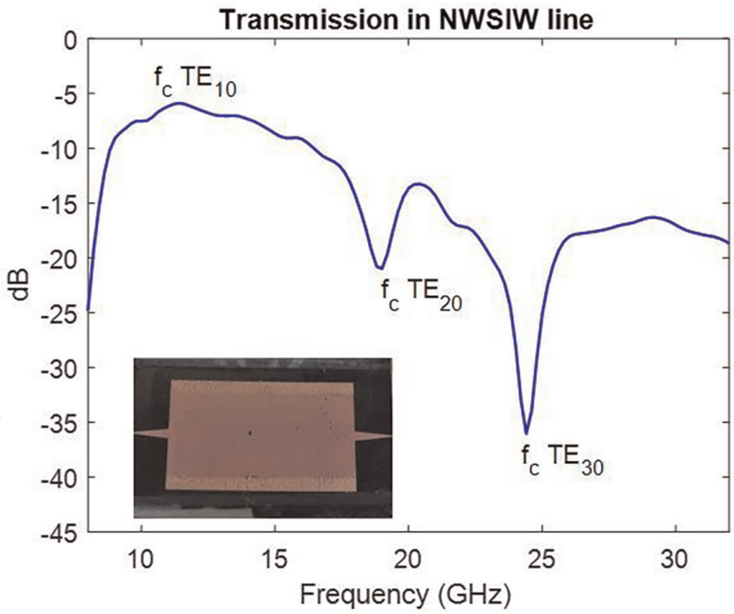

Figure 11.
Transmission measured on a NWSIW built in a 100 μm-thick AAO template. Inset shows picture of the device having width W = 6 mm.

Insert of **Figure 11** shows a picture of the fabricated NWSIW line. Material for MNW is Cu and areas filled by MNW are visible as lighter strips on upper and lower side of the brown rectangle forming the top metallization of the NWSIW, and having a length equal to 12 mm. On left- and right-hand sides of the picture taper microstrip transitions aiming at improving impedance matching are visible.

5.2 NWSIW isolator

Figure 12 shows a practical realization of a NWSIW isolator basing on the operation mode of a ferrite-slab resonant mode isolator in classical MRW technology [24, 25]. Here in order to mimick the ferrite slab, a narrow wall made of ferromagnetic NW (alloy of Nickel and iron, noted NiFe, red color) is grown close to a wall of the NWSIW (blue color), made of Cu NW grown in AAO, as shown in the inset of **Figure 12**. It has to be noted that NiFe NW forming the slab are not grown over the full height of AAO template in order to avoid the formation of a short-circuit due to contacts between conductive NiFe NW and top metallization of the waveguide, since a short-circuit would prevent the transmission of the signal.

As expected a nonreciprocal transmission is observed in the NWSIW, due to the presence of ferromagnetic material located at a specific position in the waveguide. Transmission S_{21} in forward direction is more than 10 dB lower than transmission S_{12} in reverse direction. We can conclude that the device ensures an isolation level superior to 10 dB [21], which is close to the state-of-the art, as shown in **Table 2**.

Compared to isolators based on ferrite slabs in MRW (resonant-mode isolator), the planar devices are much thinner and usually do not require an external magnetic field to bias the ferrite. The best result is obtained by Cheng et al. [26]: their planar ferrite resonance isolator is 635 μm-thick and works without DC magnetic field bias. Hemour et al. [27] propose an SIW isolator based on ferrite, with lower performances reported in **Table 2**.

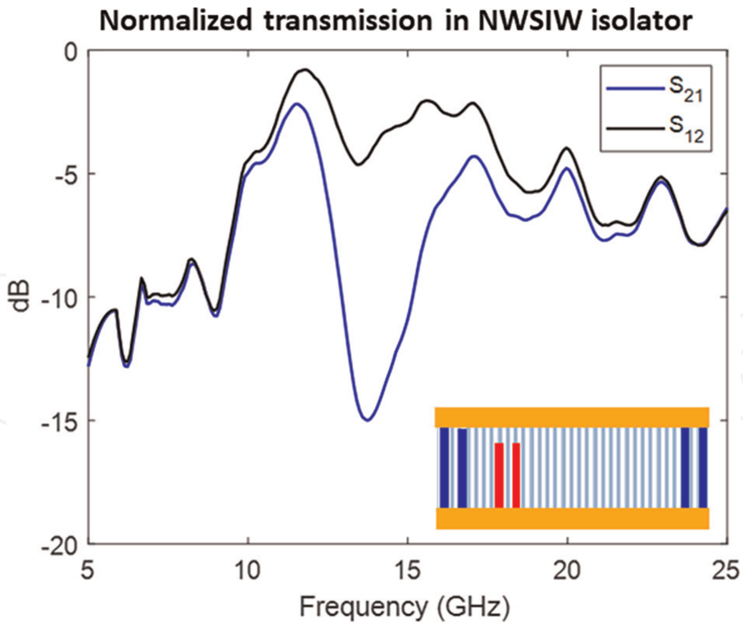

Figure 12.
Measurement of NWSIW isolator. Inset shows the topology: Cu NW (blue) form lateral walls, while NiFe NW (red) form a ferromagnetic slab. Electroplated copper metal layers (orange) form bottom and top walls of NWSIW.

Reference	Topology /technology	Material	F (GHz)	Isolation (dB/cm)	Insertion losses (dB)	Thickness (mm)
[26]	SIW in PCB	Ferrite slab	10	20	3	0.635
[27]	SIW in PCB	Ferrite slab	11	8	7	na
[28]	Microstrip on PC	Co NW	41	7	15	0.021
[29]	CPW on AAO	Ni NW	20	6.5	na	0.06
[13]	Microstrip on AAO	CoFe NW	24	14	10	0.20
[18]	NWSIW on AAO	NiFe NW	13	7	na	0.05
Figure 12 [21]	NWSIW on AAO	NiFe NW	12	11	na	0.10

Table 2.
Comparison of performances of planar SIW isolators.

The first demonstration of an isolator based on ferromagnetic nanowires (NW) was reported in [28]. Cobalt NW are included in nanoporous polycarbonate (PC) thin substrate, and 10 dB isolation is obtained, however with 15 dB insertion losses and requiring a 9 kOe DC magnetic bias. Next two other devices based on NW in AAO porous template are reported in the literature. Kuarn [29] proposed a coplanar waveguide (CPW) technology including Nickel (Ni) MNW in AAO. Reported isolation level is 6 dB/cm at 23 GHz under 5.6 kOe DC magnetic bias. The best performances for nanowire-based planar isolators were obtained by Carignan et al. [13], who measured an isolation of 14 dB/cm without DC bias on a microstrip topology including CoFeB in AAO.

Two realizations of UCLouvain combining NW in AAO and planar SIW into an NWSIW isolator are reported in the literature and do not require external DC bias. The first one [18] shows an isolation level of 7 dB/cm, while the second one [21] shown in **Figure 12** has an isolation of 11 dB/cm. These two last realizations are among the thinnest according to **Table 2**.

5.3 NWSIW EBG filter

As last illustration in this chapter, **Figure 13** presents the topology of the so-called EBG filter (for Electromagnetic Band Gap) realized in NWSIW technology. The EBG effect associated to periodic structures was introduced in the '90s [11, 30–32]. The

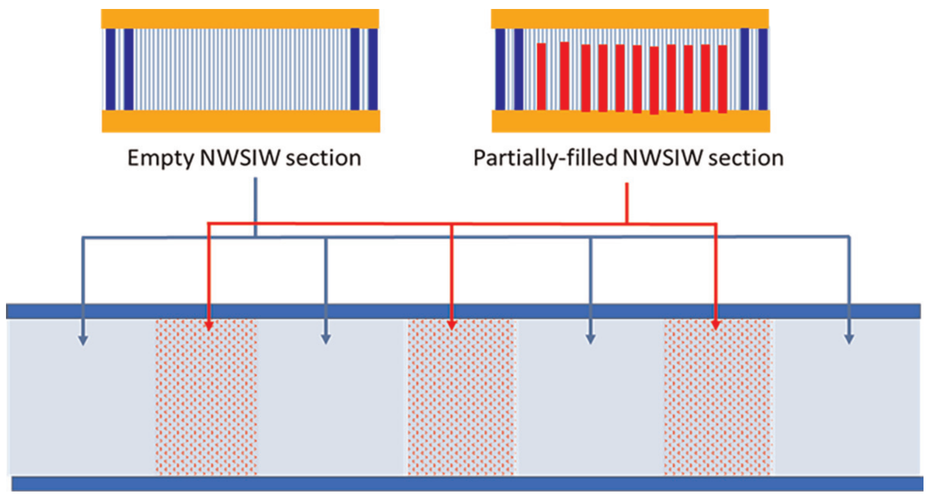

Figure 13.
Topology of EBG filter in NWSIW technology. Blue NW form vertical walls of NWSIW, while red NW having filling height h = 75% are grown in the NWSIW in order to create the EBG effect. Electroplated copper metal layers (orange) form bottom and top walls of NWSIW.

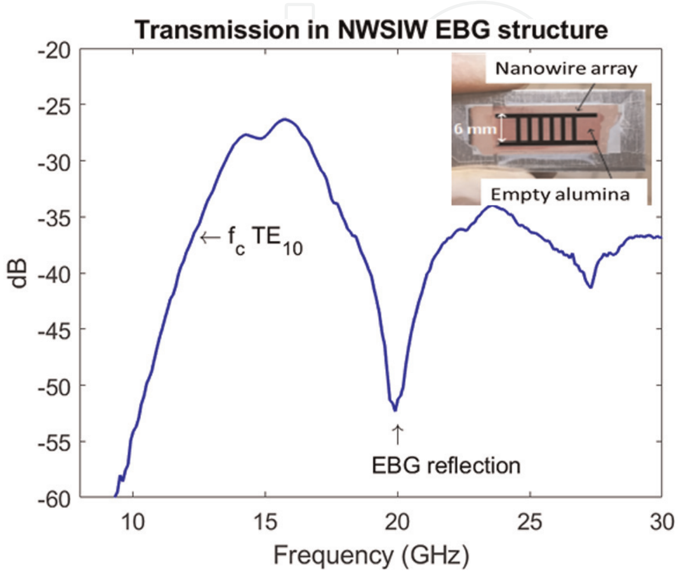

Figure 14.
Measured transmission in EBG filter in NWSIW technology. Inset: Photograph before electroplating realized at step 5 of ***Figure 10****.*

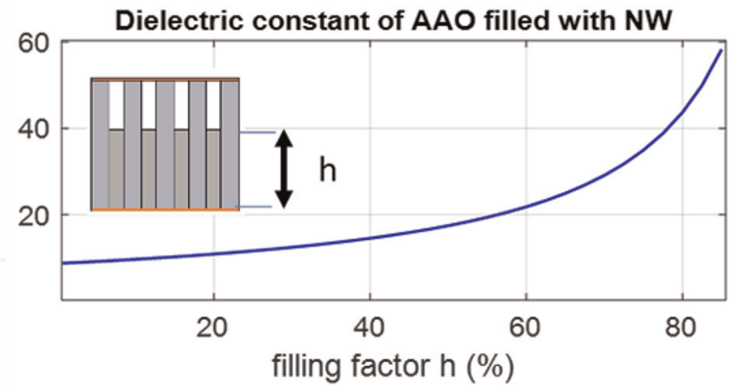

Figure 15.
Influence of filling height of NW on dielectric constant.

filter is based on the cascade of three NWSIW sections partially filled with Nickel MNW and separated by empty NWSIW sections.

Measurement of transmission in **Figure 14** shows that a gap in the transmission occurs at 20 GHz. It is created by the contrast between the dielectric constant of AAO empty sections and the much higher value of dielectric constant for sections partially filled with Ni NW over a relative filling factor h. The behavior of the dielectric constant versus h is shown in **Figure 15** and was initially introduced in [15]. The generation of the bandgap at a dedicated frequency f_o requires that the length of each section, empty and filled, is equal to a quarter wavelength at f_o. This condition is expressed by equations (7–8):

$$L_{empty\ section} = \frac{c_o}{4\, f_o\, \varepsilon_{r\ empty}} = 2.6\ \text{mm}. \tag{7}$$

$$L_{filled\ section} = \frac{c_o}{4\, f_o\, \varepsilon_{r\ filled}} = 5.1\ \text{mm} \tag{8}$$

The realized filter has a filling factor h = 75% yielding 34 as value for $\varepsilon_{r\ filled}$, while dielectric constant of empty AAO with P = 4% is close to 9.8. The contrast between dielectric constant of filled and empty sections is high and responsible for the bandgap at f_o = 20 GHz. The depth of the bandgap is −50 dB, which, compared to the maximal transmission level of - 25 dB, means a stopband rejection effect of 25 dB.

6. Challenges and perspectives of the new NWSIW technology

Coming to the end of this chapter, it is now time to conclude on the performances, the maturity and the perspectives of the NWSIW technology.

The NWSIW presented in this chapter and the classical planar SIW of **Figure 1** share about the same pros and cons:

- A fully planar geometry, based on a thin planar substrate, much more compact than classical MRW
    - The resulting disadvantage is that both topologies require specific matching structures to solve the impedance mismatch issue resulting from the low thickness of the substrate.

Reference	Topology	Technology	f (GHz)	Insertion losses (dB/cm)
[33]	CPW	NixSiy/Si	10	2
[34]	CPW	MMIC	20	5
[35]	SIW	LTCC	50	2.5
[36]	SIW	LTCC	38	4
[37]	Microstrip	NW in AAO	60	7
[38]	SIW	NW in AAO	20	7.4
[20]	NWSIW	NW in AAO	12	4.4

Table 3.
Comparison of insertion loss.

- ◦ However, the issue disappears if a whole architecture of devices is built in the same NWSIW technology on a single AAO substrate. The design can be made for a same reference impedance, so that a single transition will be needed for interfacing the designed circuit in NWSIW technology with 50 Ω reference impedance.

- An improved immunity to radiation and crosstalk interferences compared to open planar structures
  - For classical SIW, vias have to be carefully dimensioned and spaced in order to induce an efficient shield.
  - while for NWSIW a thin wall of grown nanowires is sufficient to form an efficient shield, since the nanoporous AAO template imposes a close packing of the electrodeposited MNW array.

- Compared to MRW that are empty, both SIW and NWSIW structure are filled by a medium having permittivity higher than air.
  - This reduces the size of the device for a given operational frequency
  - Devices have to cope with dielectric loss of the substrate filling the waveguide.

However, the insertion losses observed in **Figure 11** for NWSIW (8 dB at 12 GHz, corresponding to 4.4 dB/cm) are comparable or lower than other technologies/topologies, as shown **Table 3**. Insertion losses should be significantly decreased by further improvement of fabrication process. Indeed, the upper and lower Cu layers electroplated on the two faces of the AAO membrane can be thickened in order to attenuate the effect of the roughness of the metallization due its imperfect contact with porous template during step 1 and 5 of the fabrication (**Figure 10**). This will increase the shielding effect while reducing ohmic losses, in order to achieve insertion losses lower than 1 dB/cm.

The road to achieving these objectives is not actually that long. We have shown that the combination of nanowires and SIW technologies is meaningful, since it allows a facile integration of various functionalities such as filtering and nonreciprocity on a same substrate thanks to the growth of various kinds of MNW in AAO while tuning their filling height. The fabrication of a platform of miniaturized NWSIW devices that rival the state-of-the-art will be made possible by some optimizations of the fabrication process as outlined above.

Acknowledgements

The authors would like to thank Ester Tooten, Pascal Simon and Pascal Van Velthem for their help and advices.

This work was supported by the Research Science Foundation of Belgium (FRS-FNRS). Vivien VanKerckhoven acknowledges the FRS-FNRS for financial support (FRIA grant). Isabelle Huynen is Research Director of FRS-FNRS.

Nomenclature

The following abbreviations are used in this manuscript:

AAO	Anodic Aluminum Oxide
CCL	copper clad laminate
CPW	Coplanar Waveguide
Cu	Copper
EBG	Electromagnetic Band Gap
NiFe	nickel-iron alloy
MMIC	Monolithic Microwave Integrated Circuit
MNW	metallic nanowire
LTTC	Low Temperature Co-fired Ceramics
NW	Nanowire
NWSIW	Nanowired Substrate Integrated Waveguide
PCB	Printed Circuits Boards
SIW	Substrate Integrated Waveguide
UCLouvain	Université catholique de Louvain

Author details

Vivien Van Kerckhoven, Luc Piraux and Isabelle Huynen*
Université catholique de Louvain (UCLouvain), Louvain-la-Neuve, Belgium

*Address all correspondence to: isabelle.huynen@uclouvain.be

References

[1] Wu K, Deslandes D, Cassivi Y. The substrate integrated circuits - A new concept for high-frequency electronics and optoelectronics. In: Proceedings of the 6th International Conference on Telecommunications in Modern Satellite, Cable and Broadcasting Service 2003—TELSIKS 2003, Nis, Yugoslavia, 1–3 October 2003. USA: IEEE; 2003. pp. III-X. DOI: 10.1109/TELSKS.2003.1246173

[2] Pazian M, Bozzi M, Perregrini L. Crosstalk in substrate integrated waveguides. IEEE Transactions on Electromagnetic Compatibility. 2015;**57**: 80-86. DOI: 10.1109/TEMC.2014.2364634

[3] Simpson JJ, Taflove A, Mix JA, Heck H. Substrate integrated waveguides optimized for ultrahighspeed digital interconnects. IEEE Transactions on Microwave Theory and Techniques. 2006;**54**:1983-1990. DOI: 10.1109/TMTT.2006.873622

[4] Lai QH, Fumeaux C, Hong W. Mutual coupling between parallel half-mode substrate integrated waveguides. In: Proceedings of the 2012 International Conference on Microwave and Millimeter Wave Technology (ICMMT), Shenzhen, China, 5–8 May 2012. USA: IEEE; 2012. p. 4. DOI: 10.1109/ICMMT.2012.6230369

[5] Bozzi M, Georgiadis A, Wu K. Review of substrate-integrated waveguide circuits and antennas. IET Microwaves, Antennas and Propagation. 2011;**5**: 909-920. DOI: 10.1049/iet-map.2010.0463

[6] Moro R, Bozzi M, Collado A, Georgiadis A, Via S. Plastic-based substrate integrated waveguide (SIW) components and antennas. In: Proc. Eur. Microwave Integr. Circuits Conf. Amsterdam, The Netherlands, 29 Oct.-1 Nov. 2012. USA: IEEE; 2012. pp. 627-630. DOI: 10.23919/EuMC.2012.6459177

[7] Kuanr B, Veerakumar V, Marson R, Mishra SR, Kuanr AV, Camley RE, et al. Nickel nano-wires filled alumina templates for microwave electronics. IEEE Transactions on Magnetics Letters. 2009;**45**:4052-4055. DOI: 10.1109/TMAG.2009.2024880

[8] Qiao L, Han X, Gao B, Wang J, Wen F, Li F. Microwave absorption properties of the hierarchically branched Ni nanowire composites. Journal of Applied Physics. 2009;**105**:053911. DOI: 10.1063/1.3081649

[9] Chen W, Han M, Deng L. High frequency microwave absorbing properties of cobalt nanowires with transverse magnetocrystalline anisotropy. Physica B: Condensed Matter. 2010;**405**:1484-1488. DOI: 10.1016/j.physb.2009.12.026

[10] Hamoir G, Piraux L, Huynen I. Q-factor improvement of integrated inductors using high aspect ratio ferromagnetic nanowires. Microwave and Optical Technology Letters. 2012;**54**: 1484-1488. DOI: 10.1002/mop.26900

[11] Saib A, Vanhoenacker-Janvier D, Huynen I, Encinas A, Piraux L, Ferain E, et al. Magnetic photonic band-gap material at microwave frequencies based on ferromagnetic nanowires. Applied Physics Letters. 2003;**83**:2378-2380. DOI: 10.1063/1.1610798

[12] Hamoir G, De La Torre MJ, Piraux L, Huynen I. Self-biased nonreciprocal microstrip phase shifter on magnetic

nanowired substrate suitable for gyrator applications. IEEE Transactions on Microwave Theory and Techniques. 2012;**60**:152-157. DOI: 10.1109/TMTT.2012.2195016

[13] Carignan L, Caloz C, Menard D. Dual-band integrated self-biased edge-mode isolator based on the double ferromagnetic resonance of a bistable nanowire substrate. In: Microwave Theory and Techniques, Proceedings of IEEE Symposium Digest. Anaheim, CA, USA: IEEE; 2010. pp. 1336-1339. DOI: 10.1109/MWSYM.2010.5517585

[14] Saib A, Darques M, Piraux L, Vanhoenacker-Janvier D, Huynen I. An unbiased integrated microstrip circulator based on magnetic nanowired substrate. IEEE Transactions on Microwave Theory and Techniques. 2003;**83**:237. DOI: 10.1109/TMTT.2005.848818

[15] Spiegel J, De La Torre J, Darques M, Piraux L, Huynen I. Permittivity model for ferromagnetic nanowired substrates. IEEE Microwave and Wireless Components Letters. 2007;**60**: 492-494. DOI: 10.1109/LMWC.2007.899303

[16] Ramirez-Villegas R, Huynen I, Piraux L, Encinas A, De La, Torre MJ. Self-biased nonreciprocal microstrip phase shifter on magnetic nanowired substrate suitable for gyrator applications. IEEE Transactions on Microwave Theory and Techniques. 2016;**65**:72-77. DOI: 10.1109/TMTT.2012.2195016

[17] Van Kerckhoven V, Piraux L, Huynen I. A novel laser-assisted fabrication process for nanowired substrate integrated devices. In: 2018 13th European Microwave Integrated Circuits Conference (EuMIC). 23-25 Sept. 2018, Madrid, Spain. USA: IEEE; 2018. pp. 170-173. DOI: 10.23919/EuMIC.2018.8539911

[18] Van Kerckhoven V, Piraux L, Huynen I. Substrate integrated waveguide isolator based on ferromagnetic nanowires in porous alumina template. Applied Physics Letters. 2014;**105**:183107. DOI: 10.1063/1.4901277

[19] Van Kerckhoven V, Piraux L, Huynen I. A laser-assisted process to produce patterned growth of vertically aligned nanowire arrays for monolithic microwave integrated devices. Nanotechnology. 2016;**65**:72-77. DOI: 10.1088/0957-4484/27/23/235301

[20] Van Kerckhoven V, Piraux L, Huynen I. Design of substrate integrated waveguides based on nanowires: Numerical guidelines. International Journal of Numerical Modelling. 2021; **34**:e2906. DOI: 10.1002/jnm.2906

[21] Van Kerckhoven V, Piraux L, Huynen I. Fabrication of microwave devices based on magnetic nanowires using a laser-assisted process. Micromachines. 2019;**10**:475. DOI: 10.3390/mi10070475

[22] Van Kerckhoven V. Nanowire-Based Microwave Devices in Substrate Integrated Waveguide Topology Using a Laser-Assisted Fabrication Process. Louvain-La-Neuve: UCLouvain; 2019

[23] Pozar DM. Microwave Engineering. 3rd ed. Hoboken. USA: John Wiley & Sons; 2005. p. 756. DOI: 10.1002/9780470974704

[24] Schloemann E. On the theory of the ferrite resonance isolator. IRE Transactions on Microwave Theory and Techniques. 1960;**199**:605-611. DOI: 10.1109/TMTT.1960.1124723

[25] Comstock RL, Fay CE. Operation of the field displacement in rectangular waveguide isolator. IRE Transactions on Microwave Theory and Techniques. 1960;**199**:199-206. DOI: 10.1109/TMTT.1960.1124804

[26] Cheng YJ, Huang QD, Wang YR, Li JW. Narrowband substrate integrated waveguide isolators. IEEE Microwave and Wireless Components Letters. 2014;**24**:698-700. DOI: 10.1109/LMWC.2014.2344440

[27] Hemour S, Adhikari S, Ghiotto A, Wu K. Low magnetic biased SIW-based isolator: Effect of the rising temperature on the performance of the isolator. In: Proceedings of the WAMICON Conference. 6 June 2014. Tampa, USA: IEEE; 2014. p. 3. DOI: 10.1109/WAMICON.2014.6857801

[28] Spiegel J, De la Torre J, Piraux L, Huynen I. Isolator concept based on ferromagnetic nanowired substrates. In: Proceedings of International Microwave Symposium (IMS2009), June 7–12, 2009. Boston, USA: IEEE; 2006. pp. 29-32. DOI: 10.1109/MWSYM.2009.5165624

[29] Kuanr BK, Veerakumar V, Marson RL, Mishra SR, Carnley RE, Celinski Z. Nonreciprocal microwave devices based on magnetic nanowires. Applied Physics Letters. 2009;**94**:202505. DOI: 10.1063/1.3124657

[30] Yablonovitch E. Inhibited spontaneous emission in solid-state physics and electronics. Physical Review Letters. 1987;**58**:2059. DOI: 10.1103/PhysRevLett.58.2059

[31] Laso MAG, Erro MJ, Benito D, Garde MJ, Lopetegi T, Falcone F, et al. Analysis and design of 1-D photonic bandgap microstrip structures using a fiber grating model. Microwave and Optical Technology Letters. 1999;**22**:223-226. DOI: 10.1002/(SICI)1098-2760(19990820)22:4< 223: AID-MOP1>3.0.CO;2-X

[32] Sigalas MM, Soukoulis CM, Biswas R, Ho KH. Effect of the magnetic permeability on photonic band gaps. Physical Review B. 1997;**56**:959. DOI: 10.1103/PhysRevB.56.959

[33] Raman S, Rucky F, Rebeiz G. A high-performance W-band uniplanar subharmonic mixer. IEEE Transactions on Microwave Theory and Techniques. 1997;**45**:955-959. DOI: 10.1109/22.588609

[34] Kim J, Qian Y, Feng G, Ma P, Judy J, Chang MF, et al. A novel low-loss low-crosstalk interconnect for broad-band mixed-signal silicon MMIC's. IEEE Transactions on Microwave Theory and Techniques. 1999;**47**:1830-1834. DOI: 10.1109/22.788519

[35] Dancila D, Rottenberg X, Tilmans HAC, De Raedt WR, Huynen I. 57-64 GHz seven-pole bandpass filter substrate integrated waveguide (SIW) in LTCC. In: Proceedings of the 2011 IEEE MTT-S International Microwave Workshop on Millimeter Wave Integration Technologies, 15–16 September 2011; Sitges, Spain. USA: IEEE; 2011. pp. 200-203. DOI: 10.1109/IMWS3.2011.6061876

[36] Hizan HM, Ambak Z, Ibrahim A, Yusoff MZM, Kanesan T. Effect of insertion losses on millimeter-wave SIW filters using LTCC technology. In: Proceedings of the 2015 IEEE International RF and Microwave Conference (RFM 2015); 14–16 December 2015, Kuching, Malaysia. USA: IEEE; 2015. pp. 64-66. DOI: 10.1109/RFM.2015.7587714

[37] Bertrand M, Rehder GP, Serrano ALC, Gomes LG, Pinheiro JM, Alvarenga RCA, et al. Integrated

waveguides in nanoporous alumina membrane for millimeter-wave interposer. IEEE Microwave and Wireless Components Letters. 2019;**29**: 83-87. DOI: 10.1109/LMWC.2018.2887193

[38] Hamoir G. Microwave Devices Based on Unbiased Tunable Ferromagnetic Nanowire Arrays. Louvain-la-Neuve: UCLouvain; 2014